



CHORUS

This is the accepted manuscript made available via CHORUS. The article has been published as:

Effect of massive perturbers on extreme mass-ratio inspiral waveforms

Nicolás Yunes, M. Coleman Miller, and Jonathan Thornburg

Phys. Rev. D **83**, 044030 — Published 15 February 2011

DOI: [10.1103/PhysRevD.83.044030](https://doi.org/10.1103/PhysRevD.83.044030)

The Effect of Massive Perturbers on Extreme Mass-Ratio Inspiral Waveforms

Nicolás Yunes,^{1,2} M. Coleman Miller,³ and Jonathan Thornburg⁴

¹*Department of Physics and MIT Kavli Institute,*

77 Massachusetts Avenue, Cambridge, MA 02139, USA

²*Harvard-Smithsonian, Center for Astrophysics, 60 Garden St., Cambridge, MA 02138, USA*

³*Maryland Astronomy Center for Theory and Computation & Joint Space-Science Institute,
Department of Astronomy, University of Maryland, College Park, MD 20742, USA*

⁴*Department of Astronomy and Center for Spacetime Symmetries,
Indiana University, Bloomington, IN 47405, USA*

Extreme mass ratio inspirals, in which a stellar-mass object orbits a supermassive black hole, are prime sources for space-based gravitational wave detectors because they will facilitate tests of strong gravity and probe the spacetime around rotating compact objects. In the last few years of such inspirals, the total phase is in the millions of radians and details of the waveforms are sensitive to small perturbations. We show that one potentially detectable perturbation is the presence of a second supermassive black hole within a few tenths of a parsec. The acceleration produced by the perturber on the extreme mass-ratio system produces a steady drift that causes the waveform to deviate systematically from that of an isolated system. If the perturber is a few tenths of a parsec from the extreme-mass ratio system (plausible in as many as a few percent of cases) higher derivatives of motion might also be detectable. In that case, the mass and distance of the perturber can be derived independently, which would allow a new probe of merger dynamics.

I. INTRODUCTION

Space-based gravitational wave detectors such as the *Laser Interferometer Space Antenna (LISA)* are expected to see a wide variety of sources in their $\sim 10^{-4} - 10^{-1}$ Hz sensitivity band. Of these, extreme mass-ratio inspirals (EMRIs), a stellar-mass compact object (SCO) spiraling into a supermassive black hole (SMBH), are considered particularly promising because they can probe strong gravity over millions of radians of phase evolution in the last few years of evolution. As a result, EMRI waveforms serve as highly precise probes of strong gravity and of the spacetime around rotating SMBHs. Considerable study has been devoted to astrophysical scenarios for EMRIs [1–3] as well as to the analysis of their waveforms [4–10].

There has been less exploration of the possibility of deviations from isolated EMRI waveforms that might occur due to environmental effects (see e.g. [2, 11–14] for a study of differences caused by an accretion disk around the SMBH). Here we point out an effect that has not been considered in this context: the acceleration of the EMRI system by a nearby (distance of roughly a few tenths of a parsec or less) secondary SMBH. As we demonstrate, this acceleration leads to phase drifts of fractions of a radian over a year of inspiral, which is potentially detectable from EMRIs of plausible signal strength. Depending on the fraction of galaxies that merge, and on the fraction of time in such mergers that the secondary SMBH is within a few tenths of a parsec of the primary, this could affect as many as a few percent of EMRIs.

The detection of such an effect could yield a new probe of galactic merger dynamics, providing a measure of the ratio of the secondary SMBH's mass and its distance to the EMRI. If such effects are not present in a detected gravitational wave (GW), then one can place an upper limit on the density of SMBHs inside some radius of a

few tenths of a parsec. If this is the case, then one would confirm that, as far as LISA is concerned, EMRIs occur in vacuum.

This paper is organized as follows: In Sec. II we do a simple analysis of the acceleration effect as it would apply to a signal of constant frequency and amplitude, which we expand on in the Appendix. In Sec. III we explain how to model real EMRI waveforms, for the particular case of quasi-circular, equatorial orbits, and explain how to implement modifications to model an acceleration effect. In Sec. IV we extend the simple analysis of Sec. II to real waveforms and perform a dephasing and an overlap study. In Sec. V we explore whether some of these deviations can be masked by adjustments of EMRI system parameters. We present our conclusions in Sec. VI. In most of this paper, we use geometric units with $G = c = 1$. For reference, in this system of units, one solar mass $M_{\odot} = 1.476 \text{ km} = 4.92 \times 10^{-6} \text{ s}$, while $1 \text{ pc} = 1.03 \times 10^8 \text{ s} = 2.09 \times 10^{13} M_{\odot}$.

II. SIMPLE MODEL

Here we present the basic effects of acceleration in a simplified model. We assume that there is an EMRI of a SCO into a (primary) SMBH with mass M_{\bullet} on the \hat{x} - \hat{y} plane, with orbital and spin angular momentum in the \hat{z} direction. We further simplify the scenario by assuming GWs of constant frequency and amplitude. Let us also assume there is a secondary SMBH in a circular orbit about the EMRI's center of mass (COM). Suppose that the secondary SMBH has a mass M_{sec} and the total mass of the system $M_{\text{Tot}} = M_{\bullet} + M_{\text{sec}}$. Suppose also that the semi-major axis of the circular orbit of the primary-secondary SMBH system is r_{sec} , and that it is inclined to the line of sight at an angle ι (here ι is zero for a face-on

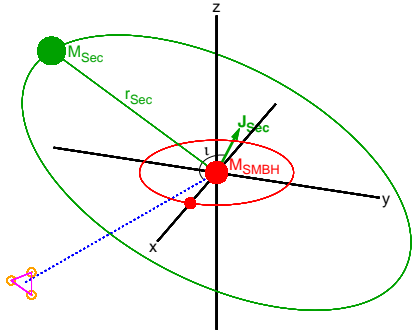


FIG. 1. Schematic view of the EMRI system (in the xy plane), the massive perturber M_{Sec} (at a distance r_{Sec} from the EMRI SMBH), and the line of sight. ι is the inclination between the primary-secondary SMBH's orbital angular momentum vector and the line of sight.

binary and 90° for an edge-on binary). We depict this scenario in Fig. 1.

If these systems are well-separated, then the EMRI's COM will move essentially at a constant velocity relative to us, with a projection into our line of sight of

$$v_{\text{los}}(t) = \left(\frac{M_{\text{Sec}}}{M_{\text{Tot}}} \right) v_{\text{Newt}} \cos(\omega_{\text{Newt}} t + \delta) \sin(\iota). \quad (1)$$

where $v_{\text{Newt}} = (GM_{\text{Tot}}/r_{\text{Sec}})^{1/2}$ is the Newtonian virial velocity, $\omega_{\text{Newt}} = (GM_{\text{Tot}}/r_{\text{Sec}}^3)^{1/2}$ is the Newtonian angular velocity for an object in a circular orbit, and δ is an initial phase, with $(\omega_{\text{Newt}} t + \delta)$ the orbital phase of the EMRI-Secondary system. A constant relative speed is entirely absorbed in a redefinition of the masses. As such, constant relative velocities cannot enter any of our results.

If the EMRI's COM is sufficiently close to the secondary SMBH, then the former will experience an measurable *acceleration*, which will produce a net Doppler phase drift relative to the best-fit waveform. Note that the orbital period for $M_{\text{Tot}} = 10^{6-7} M_\odot$ and $r_{\text{Sec}} = 0.1 - 1$ pc is at least $\sim 10^{3-5}$ years, so for the duration of a LISA observation the binary will not change phase significantly. Tidal effects on the EMRI system due to the perturber can be neglected, as this acceleration scales as the inverse cube of r_{Sec} (see Sec. IIIB for more details).

If the EMRI system is accelerated by an amount \dot{v} relative to its original line of sight speed over a time t , then the GW phase difference compared to the initial frequency is $\Delta\Phi_{\text{GW}} = \frac{1}{2}\dot{v}tN/c$, where N is the number of radians in the waveform (see Appendix A for a more detailed explanation of this effect). Let us designate by ϵ the detectable fractional phase shift: $\epsilon \equiv \Delta\Phi_{\text{GW}, \text{detect}}/N$. As a fiducial value we will use $\epsilon = 10^{-7}$, or 0.1 radians over $\sim 10^6$ radians for a typical one-year inspiral. To

leading-order in a Taylor-expansion about $\omega_{\text{Newt}} t = 0$, we then have

$$\frac{1}{2} \frac{\dot{v}t}{c} = \frac{1}{2} (\sin \iota) (\sin \delta) \frac{M_{\text{Sec}}}{r_{\text{Sec}}} \frac{t}{r_{\text{Sec}}} = \epsilon, \quad (2)$$

where we have here neglected a constant term that is non-observable. Solving for the distance at which this is satisfied gives

$$r_{\text{Sec}} \approx 0.26 \text{ pc} (\sin \iota)^{1/2} (\sin \delta)^{1/2} \left(\frac{M_{\text{Sec}}}{10^6 M_\odot} \right)^{1/2} \times \left(\frac{t}{1 \text{ yr}} \right)^{1/2} \left(\frac{\epsilon}{10^{-7}} \right)^{-1/2}. \quad (3)$$

The next order term in the phase shift scales as

$$\frac{1}{6} \frac{\ddot{v}t^2}{c} = \frac{1}{6} (\sin \iota) (\cos \delta) \frac{M_{\text{Sec}}}{r_{\text{Sec}}} \sqrt{\frac{M_{\text{Tot}}}{r_{\text{Sec}}}} \frac{t^2}{r_{\text{Sec}}^2}. \quad (4)$$

Setting this equal to ϵ and solving for r , we find

$$r_{\text{Sec}} \approx 0.025 \text{ pc} (\sin \iota)^{2/7} (\cos \delta)^{2/7} \left(\frac{M_{\text{Sec}}}{10^6 M_\odot} \right)^{2/7} \times \left(\frac{M_{\text{Tot}}}{2 \times 10^6 M_\odot} \right)^{1/7} \left(\frac{t}{1 \text{ yr}} \right)^{4/7} \left(\frac{\epsilon}{10^{-7}} \right)^{-2/7}. \quad (5)$$

Additional corrections can be computed similarly.

Therefore, for BH masses $\gtrsim 10^6 M_\odot$ and separations of a few tenths of a parsec or less, acceleration can cause a detectable shift in the simplified waveform. As we find in Sec. IV, this shift is proportional to the combination $\mathcal{A} \equiv M_{\text{Sec}}/r_{\text{Sec}}^2$. For separations of a few hundredths of a parsec or less, higher order derivatives are measurable. In this case, the detectable shift in the waveform is captured by the linear combination of \mathcal{A} and other higher-order derivative terms, such as $\mathcal{B} \equiv M_{\text{Sec}}^{3/2} r_{\text{Sec}}^{-7/2}$. Given a sufficiently small r_{Sec} one could then measure both \mathcal{A} and \mathcal{B} and thus disentangle M_{Sec} from r_{Sec} .

The range of masses and separations that could be observed, given a sufficiently strong EMRI-perturber system are depicted in Fig. 2. In this figure, we show with solid lines the constraint given by Eq. (2), and with a dashed line that of Eq. (4) (with $M_\bullet = M_{\text{Sec}}$ for simplicity), where the black, red and blue colors correspond to $\epsilon = 10^{-7}$, 10^{-6} and 10^{-5} . A larger value of ϵ corresponds to more conservative choices of what is detectable by LISA. The area above the curves show the values of M_{Sec} and r_{Sec} that could be measurable. For comparison, we also show the region of $(M_{\text{Sec}}, r_{\text{Sec}})$ space that fall in the pulsar-timing-array (PTA) sensitivity band. Of course, for PTAs to individually resolve such binaries, their distance to Earth would have to be sufficiently small [15]. In principle, however, this scenario allows for the possibility of coincident future detection of GWs with LISA and PTAs.

We now discuss the detectability of the changes discussed above for a realistic EMRI. In Sec. VI, we return to the question of how common it will be to have a secondary SMBH this close.

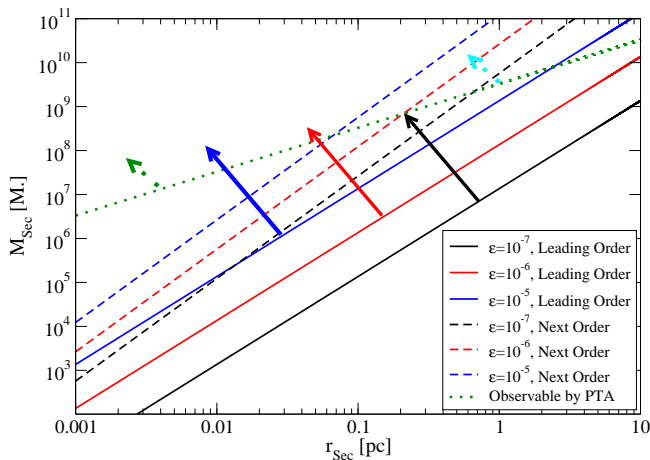


FIG. 2. Range of secondary masses and separations that could be measurable by LISA given a sufficiently strong EMRI. The region above the solid and dashed lines would be observable. Measurement of the leading-order effect gives a determination of the combination $(M_{\text{Sec}} \sin \iota)/r_{\text{Sec}}^2$, while measuring the next-order effect gives a determination of the combination $(M_{\text{Sec}} \sin \iota)^{3/2}/r_{\text{Sec}}^{7/2}$. Thus measuring both effects together allows both $M_{\text{Sec}} \sin \iota$ and r_{Sec} to be determined.

III. REALISTIC EMRI WAVEFORMS

A. Standard EOB Modeling

We employ the effective-one-body (EOB) formalism to model waveforms with and without the acceleration correction. This formalism was initially developed in [16, 17] to model comparable-mass BH binary coalescences. Improvements and extensions to other binaries were developed in [18–29] and compared to a set of numerical relativity results in [30–32] and to self-force calculations in [33, 34]. Recently, [8–10] combined the EOB approach with BH perturbation theory results to model EMRI waveforms for LISA data-analysis. We here concentrate on the formulation of [10], as it is applicable to EMRIs, the systems of interest in this paper.

We focus on quasi-circular EMRI inspirals in the equatorial plane of a spinning BH because they are simpler to model. We define the following orbital parameters: the SCO’s mass m_* ; the SMBH’s mass M_\bullet ; the total mass $M = m_* + M_\bullet$; the reduced mass $\mu = m_* m_\bullet / M$; and the symmetric mass-ratio $\nu = \mu / M$. We also assume that the EMRI’s orbital angular momentum is aligned with the MBH’s spin angular momentum $S_\bullet = a_\bullet M_\bullet = q_\bullet M_\bullet^2$, where $a_\bullet = S_\bullet / M_\bullet$ is the MBH’s spin parameter and $q_\bullet = a_\bullet / M_\bullet$ is its dimensionless spin parameter. We employ the adiabatic approximation, in which we assume that the radiation-reaction time-scale is much longer than the orbital one.

With this at hand, let us now describe the EOB approach we employ. In the adiabatic approximation, the

GW phase can be obtained by solving

$$\dot{\omega} = - \left(\frac{dE}{d\omega} \right)^{-1} \mathcal{F}(\omega), \quad (6)$$

$$\dot{\phi} = \omega, \quad (7)$$

where $\omega \equiv \dot{\phi}$ is the orbital angular frequency, with ϕ the orbital phase, overhead dots stand for time derivatives, E is the system’s total energy and \mathcal{F} is the GW energy flux. The energy of the system is [35]

$$E = M_\bullet + m_* \frac{1 - 2M_\bullet/r \pm q_\bullet M_\bullet^{3/2}/r^{3/2}}{\sqrt{1 - 3M_\bullet/r \pm 2q_\bullet M_\bullet^{3/2}/r^{3/2}}}. \quad (8)$$

where the \pm stands for prograde or retrograde orbits. In this equation and all throughout the rest of this paper, we ignore sub-leading corrections that are proportional to the EMRI’s mass-ratio. In practice, this means we ignore conservative and second-order dissipative self-force effects, i.e. the effect of the SCO on its own geometry, as well as the SCO’s spin.

The GW flux can be written in the factorized form of [10, 24, 27, 28], which in the adiabatic regime is

$$\mathcal{F}(\omega) = \frac{1}{8\pi} \sum_{\ell=2}^8 \sum_{m=0}^{\ell} (m\omega)^2 |h_{\ell m}|^2, \quad (9)$$

where the multipole-decomposed waveforms are

$$h_{\ell m}(v) = h_{\ell m}^{\text{Newt}, \epsilon_p} S_{\ell m}^{\epsilon_p} T_{\ell m} e^{i\delta_{\ell m}} (\rho_{\ell m})^\ell, \quad (10)$$

and where ϵ_p is the parity of the waveform (i.e., $\epsilon_p = 0$ if $\ell + m$ is even, $\epsilon_p = 1$ if $\ell + m$ is odd). The quantities $(S_{\ell m}^{\epsilon_p}(v), T_{\ell m}(v), \delta_{\ell m}(v)$ and $\rho_{\ell m}(v))$ in Eq. (10) can be found in [24, 27, 28]. The Newtonian waveform is

$$h_{\ell m}^{\text{Newt}, \epsilon_p} \equiv \frac{M_\bullet}{R} n_{\ell m}^{(\epsilon_p)} c_{\ell + \epsilon_p} v^{\ell + \epsilon_p} Y_{\ell - \epsilon_p, -m}(\pi/2, \phi). \quad (11)$$

where $Y_{\ell, m}(\theta, \phi)$ are spherical harmonic functions, while $n_{\ell m}^{(\epsilon_p)}$ and $c_{\ell + \epsilon_p}$ are numerical coefficients [27].

We enhance the flux of Eq. (9) by linearly adding BH absorption terms and calibration coefficients that are fitted to a more accurate, numerical flux [10]. The first modification is necessary as BHs lose energy due to GWs that both escape to infinity and fall into BHs. The second modification accounts for the fact that the bare fluxes written above are built from low-velocity (PN) expansions, and as such, are not sufficiently accurate by themselves for long evolutions, even after the resummations introduced.

The above differential system is solved with the post-circular initial conditions of [17], enhanced with a mock-evolution at $100M_\bullet$ (see e. g. [10]). The orbital phase can then be used in the waveforms of Eq. (10), together with the fact that for quasi-circular orbits

$$r = \frac{[1 - q_1(M_\bullet \omega)]^{2/3}}{(M_\bullet \omega)^{2/3}}. \quad (12)$$

where r is the EMRI's separation and $v = (M_\bullet \omega)^{1/3}$ by Kepler's third law. With the waves at hand, we then compute the GW phase and its amplitude via

$$\Phi_{\text{GW}}^{\ell m} = \Im \left[\ln \left(\frac{h_{\ell m}}{|h_{\ell m}|} \right) \right], \quad A_{\text{GW}}^{\ell m} = |h_{\ell m}|. \quad (13)$$

The GW phase as defined above needs to be unwrapped every 2π , so in practice it is simpler to define the time derivative of this quantity and then obtain $\Phi_{\text{GW}}^{\ell m}$ via integration.

B. Modifications to EOB Modeling

How do we incorporate the effects of an external acceleration into GW modeling within the EOB framework? Let us first distinguish between wave generation and wave propagation effects. By the former, we mean effects that arise in the *near-zone* (less than a gravitational wavelength away from the EMRI's COM) and that generate GWs due to the inspiral of the EMRI. By the latter, we mean effects that arise after the system has generated a GW and it propagates out to the *wave-zone*, where the observer is located, many gravitational wavelengths away from the source.

As is expected, all propagation effects, such as the backscattering (or tails) of GWs off the metric of the secondary SMBH, occur beyond Newtonian (leading) order in post-Newtonian theory [36], and can be safely neglected here. The presence of an external source, however, does introduce non-negligible modifications to the generation of GWs. One could incorporate such effects by introducing an external, vectorial force to Hamilton's equations in the direction of the perturber. This force would simply be the product of the total mass of the system and the time derivative of the velocity of Eq. (1). The modeling of this effect would require a non-adiabatic evolution, i.e. the evolution of the full set of Hamilton's equations, without assuming circular orbits or using Kepler's third law. One expects that such force would induce eccentricity and inclination in the inspiral, driving the SCO out of the equatorial plane of the secondary SMBH.

One can estimate the magnitude of this effect by considering the tidal force effect of the perturber on the COM relative to the SCO's acceleration due to the secondary SMBH. Since the tidal force scales as $F_{\text{Tidal}} = M_{\text{Sec}}/r_{\text{Sec}}^3$, this effect is suppressed relative to the acceleration by a factor of $r/r_{\text{Sec}} \sim 10^{-4}$ for an EMRI with orbital separation of $30m_\bullet$ and a primary-secondary SMBH orbital separation of 0.01 pc. The ratio is this small because the perturber is assumed to be at parsec scales away from the COM, and one parsec translates to $\sim 10^{13}M_\odot$ in geometric units. Since the tidal force scales as the inverse of the separation cubed, any tidal effects are insignificant.

Given that this type of generation effects are suppressed, are there any others that should be included?

The dominant generation effect is simply a Doppler shift in the frequencies, which then leads to an integrated modification in the GW phase (see the Appendix for a detailed explanation of this Doppler effect). In this sense, such a correction is similar to the integrated Sachs-Wolfe effect for GWs [37], where here the perturbation to the potential is given by a third body, instead of some cosmological background. The implementation of this correction to an EOB evolution is simple: divide the right-hand-side of Eq. (7) by the appropriate Doppler factor

$$\dot{\phi} = \omega \quad \rightarrow \quad \dot{\phi} = \omega [1 + v_{\text{los}}(t, \delta = \pi/2)]. \quad (14)$$

In this equation, we have not included the appropriate Lorentz factor Γ , since $v_{\text{Newt}}/c \ll 1$, and we can linearize in this quantity. Moreover, we have removed the constant velocity drift component of v_{los} by choosing $\delta = \pi/2$, as the former is not measurable.

IV. PERTURBING ACCELERATION EFFECT ON RELATIVISTIC EMRI WAVEFORMS

A. Preliminary Considerations

With the machinery described in Sec. III, we can construct modified EMRI waveforms as a function of time, for a given value of the second MBH mass and separation to the EMRI's COM. We consider the following two EMRI systems, integrated for one year each:

- **System I:** The primary SMBH has mass $m_\bullet = 10^5 M_\odot$ and spin parameter $q_\bullet = 0.9$, while the SCO has mass and spin parameter $m_\star = 10 M_\odot$ and $q_\star = 0$. This system inspirals for $\sim 6 \times 10^5$ rads of orbital phase between orbital separations $r/M \in (16, 26)$. In this range the orbital velocities are $v \in (0.2, 0.25)$ and the GW frequencies are $f_{\text{GW}} \in (0.005, 0.01)$ Hz.
- **System II:** The primary SMBH has mass $m_\bullet = 10^6 M_\odot$ and spin parameter $q_\bullet = 0.9$, while the SCO has mass and spin parameter $m_\star = 10 M_\odot$ and $q_\star = 0$. This system inspirals for $\sim 3 \times 10^5$ rads of orbital phase between orbital separations $r/M \in (11, r_{\text{ISCO}})$. In this range the orbital velocities are $v \in (0.3, v_{\text{ISCO}})$ and the GW frequencies are $f_{\text{GW}} \in (0.001, f_{\text{GW}}^{\text{ISCO}})$ Hz.

System I exits the most sensitive part of the LISA band at around $16M$, which is why we stop the evolution there. In contrast, Sys. II is stopped when the SCO reaches the innermost stable circular orbit (ISCO). For each of these systems, we explore a variety of secondary SMBH masses $M_{\text{Sec}} = (10^5, 10^6)M_\odot$ as well as a variety of separations $r_{\text{Sec}} = (0.01, 0.1, 1)$ pc. Larger secondary masses are also possible; these would have equivalent effects on the EMRI at correspondingly larger distances $r \sim M^{1/2}$. (For example, $M_{\text{Sec}} = 10^9 M_\odot$ at $r = 30$ pc would have

m_\bullet	m_\star	M_{Sec}	r_{Sec}/pc	T_{Orb}^\star	T_{Orb}^\bullet	T_{GW}^\star	T_{GW}^\bullet
10	10^5	10^5	10^{-2}	10^{-5}	2.1×10^2	5.6	10^{19}
10	10^5	10^5	10^{-1}	10^{-5}	6.6×10^3	5.6	10^{23}
10	10^5	10^5	10^{+0}	10^{-5}	2.1×10^5	5.6	10^{27}
10	10^5	10^6	10^{-2}	10^{-5}	8.9×10^1	5.6	10^{18}
10	10^5	10^6	10^{-1}	10^{-5}	2.8×10^3	5.6	10^{22}
10	10^5	10^6	10^{+0}	10^{-5}	8.9×10^4	5.6	10^{26}
10	10^6	10^5	10^{-2}	10^{-5}	8.9×10^2	18	10^{18}
10	10^6	10^5	10^{-1}	10^{-5}	2.8×10^3	18	10^{22}
10	10^6	10^5	10^{+0}	10^{-5}	8.9×10^4	18	10^{26}
10	10^6	10^6	10^{-2}	10^{-5}	6.6×10^2	18	10^{18}
10	10^6	10^6	10^{-1}	10^{-5}	2.1×10^3	18	10^{22}
10	10^6	10^6	10^{+0}	10^{-5}	6.6×10^4	18	10^{26}

TABLE I. Summary of System properties. All masses are in units of M_\odot , r_{Sec} is in units of parsecs and all time scales are in units of years. The time to merger is here estimated as $T_{\text{GW}} = r/\dot{r}_{\text{GW}}$, where \dot{r}_{GW} is the rate of change of the orbital separation due to GW emission and for r we take the values in the itemized list. The superscript star stands for quantities associated with the SCO-SMBH system, while the solid dot stands for those associated with the SMBH-SMBH system.

equivalent effects to $M_{\text{Sec}} = 10^6 M_\odot$ at $r = 1$ pc.) All of this information is summarized in Table I, including the orbital periods T_{Orb} and the time to merger due to GW emission T_{GW} . In all cases we set $\sin \iota = 1$ and $\delta = \pi/2$, as this leads to the largest possible effect. The reasoning behind this is that if this effect is not observable with this choice of parameters, it will not be observable with any other choice.

B. Dephasing Study

Let us define the dephasing between waveforms as follows:

$$\Delta\Phi_{\text{GW}} \equiv \Phi_{\text{GW}}^{\text{Acc}} - \Phi_{\text{GW}}^{\text{no. Acc}} \quad (15)$$

where $\Phi_{\text{GW}}^{\text{Acc}}$ is the GW phase of an EMRI waveform with an accelerated COM, while $\Phi_{\text{GW}}^{\text{no. Acc}}$ is that of an inertial COM. We have here aligned the waveforms in time and phase before computing this dephasing. This alignment is equivalent to minimizing the statistic in Eq. (23) of [31], which in turn is the same as maximizing the fitting factor over time and phase of coalescence in a matched filtering calculation with white noise [31]. The alignment is done here in the same way as in [8–10].

Figure 3 plots the dephasing of the dominant $(\ell, m) = (2, 2)$ GW mode as a function of time in months for Sys. I and II. The different line colors/shades correspond to different separations to the perturber [$r_{\text{Sec}} = (0.01, 0.1, 1)$ pc], while different line styles correspond to different perturber masses [$M_{\text{Sec}} = (10^5, 10^6)M_\odot$]. Observe that for both Systems a dephasing of order 0.1 rads is achieved for separations $r_{\text{Sec}} \lesssim 0.1$ pc over less than one year. This is consistent with the estimates of Sec. II. Similarly, more

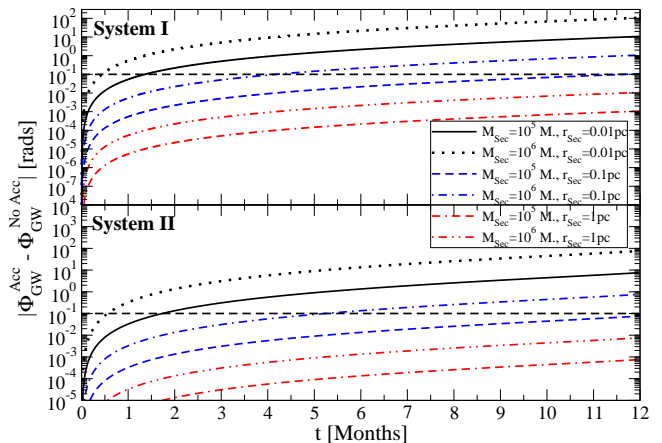


FIG. 3. Dephasing for Sys. I and II as a function of time in units of months, for a variety of separations and masses of the perturber.

massive perturbers enhance the dephasing roughly by one order of magnitude.

The amplitudes of the waveforms are not shown in this figure; they disagree at the level of 10^{-3} for Sys. I and 10^{-4} for Sys. II.

The magnitude and shape of the dephasing depends on how far away and massive the perturber is. One can show that the dephasing scales as $\Delta\Phi_{\text{GW}} \propto NM_{\text{Sec}}T/r_{\text{Sec}}^2$, where T is the observation time and N is the number of cycles. Since there is a factor of two fewer GW cycles in Sys. II relative to Sys. I, then the dephasing for the former is also smaller by a factor of two.

C. Overlap Study

The dephasing study of the previous subsection is suggestive, but not sufficiently quantitative to assess whether such types of corrections are large enough to be measurable. Let us then perform a slightly more sophisticated data analysis study here.

Given any time series $A(t)$ and $B(t)$, one can construct the inner-product

$$(A|B) = 4 \text{Re} \int_0^\infty \frac{\tilde{A}(f) \tilde{B}^*(f)}{S_n(f)} df \quad (16)$$

where the overhead tildes stand for the Fourier transform, the star stands for complex conjugation and $S_n(f)$ is the spectral density of noise in the detector. We choose here the sky-averaged version of the noise curve presented in [38, 39].

With this inner-product, we can now construct some data analysis measures. The signal to noise ratio (SNR) of signal A is

$$\rho(A) = \sqrt{(A|A)}, \quad (17)$$

while the overlap between signals a and b is

$$M = \max \frac{(A|B)}{\sqrt{(A|A)(B|B)}}. \quad (18)$$

with the mismatch $MM = 1 - M$. The max label in Eq. (18) is to remind us that this statistic must be maximized over an event time (e.g., the time of coalescence of the EMRI system) and a phase shift [26]. If the overlap is larger than 97% (or equivalently, if the mismatch is lower than 3%), then the difference between waveforms A and B is sufficiently small to not matter for detection purposes (see e. g. [40]). The minimum overlap quoted above (97%) is mostly conventional, motivated by the fact that the event rate scales as the cube of the overlap for a reasonable source distribution. For an overlap larger than 97%, no more than 10% of events are expected to be lost at SNRs of $\mathcal{O}(10)$. Of course, for larger SNRs, one might not need such high overlaps, although EMRI sources are expected to have SNRs < 100 .

Whether the difference between waveforms A and B can be detected in parameter estimation can be assessed by computing the SNR of the difference in the waveforms $\delta h \equiv A - B$:

$$\rho(\delta h) = \sqrt{(\delta h|\delta h)} = 4 \operatorname{Re} \int_0^\infty \frac{\tilde{\delta h}(f) \tilde{\delta h}^*(f)}{S_n(f)} df. \quad (19)$$

When this SNR equals unity, then one can claim that A and B are sufficiently dissimilar that they can be differentiated via matched filtering (see e. g. [41]).

We applied these measures to EOB waveforms with and without acceleration of the COM. The results are plotted in Fig. 4 as a function of observation time in months. The vertical dotted lines correspond to observation times of (0.5, 2, 4, 6, 9, 12) months, and the numbers next to them, in parenthesis, stand for the SNR of Sys. I and II for that observation time. The different line styles and colors correspond to mismatches and SNRs of the error for different secondary systems. Observe that the mismatch is always smaller than 0.03 (the solid black horizontal line), suggesting that this effect will not affect detection. Observe also that the SNR of the difference reaches unity (the dashed black horizontal line) in between 6 and 12 months of observation, and for the $M_{\text{Sec}} = 10^6 M_\odot$, $\rho(\delta h)$ reaches ~ 10 after one year. This suggests that given a sufficiently strong EMRI with SNR $\sim 50 - 100$, the magnitude of this effect is in principle detectable within one year of coherent integration.

V. DEGENERACIES

Now that we have determined that there exists a set of plausible perturber parameters for which the magnitude of the correction could be measurable, let us consider the possibility of degeneracies. That is, let us investigate whether we can mimic an acceleration of the

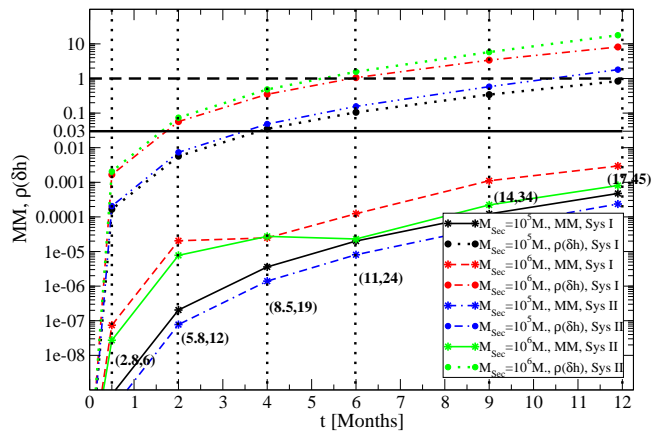


FIG. 4. Mismatch as a function of time in units of months for Sys. I and II and different perturber masses, all at a separation of $r_{\text{Sec}} = 0.1$ pc. SNRs for Sys. I and II are given in parentheses for a source at 1 Gpc.

COM by changing the intrinsic parameters (the component masses, the spin parameter, etc.) in the non-accelerating waveform. The simplest way to see whether this is possible is to study the frequency dependence of the GW modification introduced by the COM's acceleration.

Let us then remind ourselves of how the frequency-domain representation is constructed. For this, we employ the stationary-phase approximation (see e. g. [42]), under which, the frequency-domain waveform is simply

$$\tilde{h}(f) = \mathcal{A} f^{-7/6} e^{i\psi(f)}, \quad (20)$$

where the Newtonian (leading-order) amplitude is $\mathcal{A} = \pi^{-2/3} 30^{-1/2} \mathcal{M}^{5/6} D_L^{-1}$, with $\mathcal{M} = \eta^{3/5} M$, while the phase is constructed from

$$\psi(f) = -\frac{\pi}{4} + 2\pi f t(f) - 2\phi(f), \quad (21)$$

where the second term arises due to the Fourier transform and the third term due to the oscillatory nature of the time-domain waveform.

The phase of the frequency-domain waveform in the stationary phase approximation is then controlled by these last two terms in Eq. (21). The first term can be computed via

$$2\pi f t(f) = 2\pi f \int^{f/2} \frac{\tau(F')}{F'} dF', \quad (22)$$

where f is the GW frequency, while the second term can be calculated from

$$\phi(f) = 2\pi \int^{f/2} \tau(F') dF', \quad (23)$$

where $\tau(F) \equiv F/\dot{F}$ and F is the orbital frequency.

The Doppler correction to the waveform comes in the calculation of $\phi(f)$, as this is simply the integral of the

frequency. For simplicity, we can reparameterize the $v_{\text{los}}(t) \rightarrow v_{\text{los}}(F)$, by noting that, to Newtonian order,

$$2\pi F(t) = \frac{4^{-3/2}}{M} \left[\frac{\eta}{5M} (t_c - t) \right]^{-3/8}, \quad (24)$$

which we can invert to obtain

$$t(F) = t_c - \frac{5M}{256\eta} (2\pi MF)^{-8/3}, \quad (25)$$

where t_c is the time of coalescence of the EMRI system. Taylor-expanding Eq. (1) about $\omega_{\text{Newt}} t = 0$, we find

$$v_{\text{los}} \sim v_0 + v_1 (2\pi MF)^{-8/3} + v_2 (2\pi MF)^{-16/3} + v_3 (2\pi MF)^{-8}, \quad (26)$$

where the v_i coefficient are the following frequency-independent functions:

$$\begin{aligned} v_0 &= \left(\frac{M_{\text{Sec}}}{M_{\text{Tot}}} \right)^{1/2} \left(\frac{M_{\text{Sec}}}{r_{\text{Sec}}} \right)^{1/2} \left[\cos \delta - \left(\frac{M_{\text{Tot}}}{r_{\text{Sec}}} \right)^{1/2} \frac{t_c}{r_{\text{Sec}}} \sin \delta \right. \\ &\quad \left. - \frac{1}{2} \frac{M_{\text{Tot}} t_c^2}{r_{\text{Sec}}^3} \cos \delta + \frac{1}{2} \left(\frac{M_{\text{Tot}}}{r_{\text{Sec}}} \right)^{3/2} \frac{t_c^3}{r_{\text{Sec}}} \sin \delta \right] \sin \iota \\ v_1 &= \frac{10}{512} \frac{M M_{\text{Sec}}}{r_{\text{Sec}}^2} \eta^{-1} (\sin \iota) \left[\sin \delta + \left(\frac{M_{\text{Tot}}}{r_{\text{Sec}}} \right)^{1/2} \frac{t_c}{r_{\text{Sec}}} \cos \delta \right. \\ &\quad \left. - \frac{1}{2} \frac{M_{\text{Tot}} t_c^2}{r_{\text{Sec}}^3} \sin \delta \right] \\ v_2 &= \frac{25}{131072} \frac{M^2 M_{\text{Sec}}}{r_{\text{Sec}}^3} \left[- \left(\frac{M_{\text{Tot}}}{r_{\text{Sec}}} \right)^{1/2} \cos \delta + \frac{M_{\text{Tot}} t_c}{r_{\text{Sec}}^2} \sin \delta \right] \\ &\quad \times \eta^{-2} \sin \iota, \\ v_3 &= - \frac{125}{100663296} \frac{M^3 M_{\text{Sec}} M_{\text{Tot}}}{r_{\text{Sec}}^5} \eta^{-3} \sin \delta \sin \iota. \end{aligned} \quad (27)$$

Notice that v_0 is of $\mathcal{O}(M^{1/2}/r_{\text{Sec}}^{1/2})$, v_1 is of $\mathcal{O}(M^2/r_{\text{Sec}}^2)$, v_2 is of $\mathcal{O}(M^{7/2}/r_{\text{Sec}}^{7/2})$ and v_3 is of $\mathcal{O}(M^5/r_{\text{Sec}}^5)$.

With these relations at hand, we can now compute the correction to the frequency-domain waveform phase in the stationary phase approximation. Denoting by $\Delta\psi = \psi_{\text{Acc}} - \psi_{\text{no. Acc}}$, we find that

$$\begin{aligned} \Delta\psi &= -4\pi \int^{f/2} \tau(F') v_{\text{los}}(F') dF', \\ &\sim -\frac{5\pi}{24} \frac{M}{\eta} \int^{f/2} (2\pi MF')^{-8/3} \left[v_0 + v_1 (2\pi MF')^{-8/3} \right. \\ &\quad \left. + v_2 (2\pi MF')^{-16} + v_3 (2\pi MF')^{-8} \right] dF' \end{aligned} \quad (28)$$

where in the second line we have used that to Newtonian order

$$\dot{F} = \frac{48}{5\pi M^2} (2\pi MF)^{11/3}. \quad (29)$$

Normalizing this phase correction by the Newtonian form of the frequency-domain waveform phase, we find

$$\begin{aligned} \Delta\psi &= \frac{3}{128} (\pi \mathcal{M} f)^{-5/3} \left[\frac{8}{3} v_0 + \frac{40}{39} v_1 \eta^{8/5} (\pi \mathcal{M} f)^{-8/3} \right. \\ &\quad \left. + \frac{40}{63} v_2 \eta^{16/5} (\pi \mathcal{M} f)^{-16/3} + \frac{40}{39} v_3 \eta^{24/5} (\pi \mathcal{M} f)^{-8} \right] \end{aligned} \quad (30)$$

Setting $\delta = \pi/2 = \iota$, the above expression simplifies to

$$\begin{aligned} \Delta\psi &= \frac{3}{128} (\pi \mathcal{M} f)^{-5/3} \left[-\frac{8}{3} \frac{M_{\text{Sec}} t_c}{r_{\text{Sec}}^2} + \frac{4}{9} \frac{M_{\text{Sec}} M_{\text{Tot}} t_c^2}{r_{\text{Sec}}^5} \right. \\ &\quad \left. + \left(\frac{25}{1248} \frac{\mathcal{M} M_{\text{Sec}}}{r_{\text{Sec}}^2} - \frac{25}{2496} \frac{\mathcal{M} M_{\text{Sec}} M_{\text{Tot}} t_c^2}{r_{\text{Sec}}^5} \right) (\pi \mathcal{M} f)^{-8/3} \right. \\ &\quad \left. + \frac{125}{1032192} \frac{M^2 M_{\text{Sec}} M_{\text{Tot}} t_c}{r_{\text{Sec}}^5} (\pi \mathcal{M} f)^{-16/3} \right. \\ &\quad \left. - \frac{625}{1094713344} \frac{M^3 M_{\text{Sec}} M_{\text{Tot}}}{r_{\text{Sec}}^5} (\pi \mathcal{M} f)^{-8} \right]. \end{aligned} \quad (31)$$

Let us now discuss this result in more detail. The first two terms inside the square bracket in Eq. (31) arise due to a constant misalignment between the time of coalescence of the EMRI system and the primary-secondary SMBH system (we have implicitly set the latter to zero). This effect can be absorbed via a redefinition of the chirp mass, and thus, it is not observable. All other lines in Eq. (31), on the other hand, contain a non-trivial frequency-dependence and they cannot be reabsorbed via a redefinition of intrinsic parameters.

A physical way to think about this is the following. Given a signal and a template without modeling a secondary perturber, one would like to maximize the phase coherence by shifting the template's phase and frequency. Such a shift corresponds to an adjustment of the total mass and the chirp mass, which eliminates the first term in Eq. (31). Once this shift is done, however, there are no other template parameters that can be shifted, while the frequency derivatives of the signal and template will continue to disagree.

The many terms that arise in the second, third and fourth lines of Eq. (31) are due to the Taylor expansion in $\omega_{\text{Newt}} t$, which in frequency space has become an expansion in inverse powers of $(M f)$ and $(r_{\text{Sec}}/M_{\text{Sec}})$. Clearly, the second line Eq. (31) is dominant over all others as it scales with r_{Sec}^{-2} to leading order, while the third and fourth lines scale as r_{Sec}^{-5} . If $M_{\text{Sec}}/r_{\text{Sec}}$ is large enough, however, one might be able to measure the coefficients in front of both the dominant $f^{-8/3}$ term and the $f^{-16/3}$ or f^{-8} term. This would then imply that one could break the degeneracy between M_{Sec} and r_{Sec} in the leading order term and measure both quantities.

Ignoring such possible acceleration effects could introduce a bias in the extraction of parameters via matched filtering [43, 44]. Imagine, for example, that an EMRI GW is detected with vacuum templates. One would then proceed to extract parameters from this detection, such as the primary SMBH's and SCO's mass with some error

bars. Usually, the error estimate accounts for statistical error plus possible systematics with the modeling. The acceleration effect here would be one such systematic, whose magnitude would have to be determined via a careful Markov-Chain Monte-Carlo exploration of the likelihood surface.

Notice also that in Eq. (31) we have kept only the Newtonian contribution to an infinite post-Newtonian expansion. This is essentially because in Eqs. (24) and (29) we have dropped all but the leading order, Newtonian term. Interestingly, the correction terms that arise at leading order are dominant over the Newtonian piece, as they depend on high inverse powers of frequency (in particular, higher than $5/3$). This implies that if a detailed parameter estimation study were to be carried out, these post-Newtonian terms should be taken into account, as they contribute at the same order as the Newtonian term in an inertial frame.

The dependence of the correction in Eq. (31) on different powers of the frequency suggests that these terms are non-degenerate with the standard ones that appear in the non-accelerating GW phase. More precisely, the GW phase in an inertial frame is given by (see eg. [42]).

$$\psi(f)_{\text{no. Acc}} = 2\pi f t_c - \phi_c + \frac{3}{128} (\pi \mathcal{M} f)^{-5/3} \quad (32)$$

$$\times \left[1 + \left(\frac{3715}{756} + \frac{55}{9} \eta \right) \eta^{-2/5} (\pi \mathcal{M} f)^{2/3} + \dots \right],$$

where ϕ_c is the phase of coalescence and the ellipses stand for higher order terms in the post-Newtonian series. Notice that there are no powers of $f^{-8/3}$, $f^{-16/3}$ or f^{-8} in the above equation. Thus, the correction computed in Eq. (31) is weakly correlated to the GW phase in an inertial frame, i. e. the off-diagonal elements of the Fisher matrix are small for the $M_{\text{sec}}/r_{\text{sec}}^2$ coordinate sector relative to the diagonal term. Although these results are suggestive, a more detailed analysis should be carried out to determine the level of correlation between all parameters and the accuracy to which M_{sec} and r_{sec} could be extracted.

Although the correction due to the acceleration of the COM seems to be weakly correlated to other intrinsic parameters, one might wonder whether it is degenerate with other effects not included in vacuum GR waveforms. Takahashi and Nakamura [45] have studied the effect of the acceleration of the Universe in the frequency-domain form of the waveform. They find that

$$\Delta\psi = \frac{3}{128} (\pi \mathcal{M} f)^{-5/3} \left[\frac{25}{768} \mathcal{M} \dot{z} (\pi \mathcal{M} f)^{-8/3} \right]. \quad (33)$$

One can clearly see that this cosmological effect is degenerate with the one computed here [the second line in Eq. (31)]. However, the magnitude of Eq. (33) is much smaller than that of Eq. (31), simply because $H_0 \ll M_{\text{sec}}/r_{\text{sec}}^2$ for all relevant perturbers considered here. For example, at small redshift, $H_0 \sim 10^{-23} \text{ km}^{-1}$ in geometric units, while at $r_{\text{sec}} = 0.1 \text{ pc}$ and for a $10^6 M_\odot$

perturber, $M_{\text{sec}}/r_{\text{sec}}^2 \sim 10^{-19} \text{ km}^{-1}$. The perturber separation at which these effects become comparable is approximately $r_{\text{sec}} \sim 11 \text{ pc}$ [$M_{\text{sec}}/(10^6 M_\odot)$] $^{1/2}$.

Another possible source of degeneracy could be if there are corrections to general relativity that induce phase modifications with the specific frequency dependence found in Eq. (31). In fact, we see that the result obtained here can be mapped to the parameterized post-Einsteinian framework [44] with the choice

$$\alpha = 0, \quad \beta = \frac{25}{1248} \frac{M_{\text{sec}} \mathcal{M}}{r_{\text{sec}}}, \quad b = -\frac{8}{3}, \quad (34)$$

to leading order in $M_{\text{sec}}/r_{\text{sec}}$ (see e.g. Eq. 1 in [44]). As found in that paper, however, there are no known alternative theories to date that could potentially lead to the frequency dependence found in Eq. (31).

VI. DISCUSSION AND CONCLUSIONS

We have shown that a $\sim 10^6 M_\odot$ secondary SMBH within a few tenths of a parsec of the EMRI system can produce detectable modifications in the waveform. A more massive secondary SMBH at a correspondingly larger distance would produce equivalent effects. It is not possible to say with certainty how common this will be. A rough upper limit can be obtained from the following observation. Since a redshift of $z = 1$ (corresponding roughly to 10^{10} years), tens of percent of Milky Way-like galaxies have had a major merger [46, 47]. If the typical merger takes hundreds of millions of years, then at most a few percent will be involved in a merger at any stage. The fraction of time spent at separations $\lesssim 1 \text{ pc}$ remains uncertain; although there are well-understood dynamical processes that can reduce the secondary SMBH's separation to $\sim 1 \text{ pc}$ and gravitational radiation will bring the binary to merger from $\sim 10^{-3} \text{ pc}$, the transition between the regimes is uncertain (this is commonly called the ‘‘final parsec problem’’; see, e.g., [48] for a discussion). It is therefore possible that the system spends considerable time at roughly the detectable separations.

We also note that when a secondary SMBH comes within a few tenths of a parsec of the primary, various dynamical effects temporarily increase the rate of close encounters of stellar-mass objects with both SMBHs [49]. As a result, it may be that a disproportionate number of EMRIs occur with a secondary SMBH nearby. Indeed, recently [50] estimated that more than 10% of all tidal disruption events could originate in massive black hole binaries, so if the EMRI fraction is similar it corresponds to our rough estimate.

In these cases, measurement of an EMRI phase shift affords a new way to detect the presence of a binary SMBH. If the separation is close enough to measure an additional derivative of the motion, then the degeneracy between the secondary mass and its distance is broken. If the EMRI-SMBH system is sufficiently close, then pulsar timing measurements [15] might also be able to detect

gravitational waves from the SMBH-SMBH binary. Alternatively, if no phase shift is detected, then this implies that there are no secondary SMBH in a radius of a few tenths of a parsec, thus implying an upper limit on the density of BHs close to the detected EMRIs. In principle, therefore, EMRIs have another astrophysical link in addition to their utility in testing general relativity.

The importance of the astrophysical environment in EMRI GW modeling is a double-edged sword. Although on the one hand, one could potentially extract some astrophysical information, on the other, these effects could make it difficult to test general relativity [44]. For such tests to be possible, one must have complete control of the waveforms within general relativity. If the astrophysical environment needs to be included, then the modeling might be dramatically more difficult. We note here, however, that only a fraction of EMRIs would experience the astrophysical environment effect discussed here. If deviations from general relativity are present, on the other hand, these should be present for all EMRIs. Thus, in principle, a statistical analysis would allow us to disentangle deviations in our waveforms to discern whether they have an astrophysical or theoretical origin.

ACKNOWLEDGMENTS

We are grateful to Pau Amaro-Seoane and Ed Porter for organizing the Astro-GR workshop in Paris, where this idea was conceived. We are also grateful to Bence Kocsis and to the anonymous referee for many useful comments and suggestions. MCM acknowledges support from NASA grant NNX08AH29G. NY acknowledges support from NASA through the Einstein Postdoctoral Fellowship Award Number PF0-110080 issued by the Chandra X-ray Observatory Center, which is operated by the Smithsonian Astrophysical Observatory for and on behalf of NASA under contract NAS8-03060.

Appendix A: Acceleration Effect

Here we explain in more detail how the Doppler correction to the waveform comes about. Let us consider the effect of an acceleration on the COM position vector. For simplicity we consider the toy-model of a perfect circular orbit with angular velocity ω , whose position vector in the COM can be parameterized as

$$\vec{x} = b(\cos\omega t, \sin\omega t, 0), \quad (\text{A1})$$

where b is the binary's separation and we have erected a Cartesian coordinate system, with the binary in the \hat{x} - \hat{y} plane. If an external force is present that causes an acceleration, this in turn will cause a displacement $\vec{x} \rightarrow \vec{x}' = \vec{x} + \delta\vec{x}$. Let us parameterize the magnitude of this displacement as $|\delta\vec{x}| = (1/2)\dot{v}_{\text{los}}t^2$, which holds to Newtonian order for a uniformly accelerated body. One

can then show that the shift in the magnitude of the COM velocity vector is simply

$$|\vec{v}'| = |\vec{v}| + \frac{1}{2}\dot{v}_{\text{los}}t(\hat{x} \cdot \delta\hat{x}) + \mathcal{O}(\dot{v}_{\text{los}}^2 t^2), \quad (\text{A2})$$

where $\dot{v} = \dot{\vec{x}}$ is the unperturbed velocity vector. Notice that there is a factor of 1/2 here, just as in the estimates of Sec. II.

Before proceeding, it is useful to concentrate on this velocity shift. Choosing $\delta = \pi/2 = \iota$, one can easily show that

$$v_{\text{los}} \sim \frac{M_{\text{Sec}}}{M_{\text{Tot}}} v_{\text{Newt}}(\omega_{\text{Newt}} t) \left[1 - \frac{1}{6}\omega_{\text{Newt}}^2 t^2 + \mathcal{O}(\omega_{\text{Newt}}^4 t^4) \right], \quad (\text{A3})$$

upon Taylor expanding about $\omega_{\text{Newt}} t \ll 1$. We can take the time-derivative of v_{los} and then Taylor-expand again to find:

$$\dot{v}_{\text{los}} t \sim -\frac{M_{\text{Sec}}}{M_{\text{Tot}}} v_{\text{Newt}}(\omega_{\text{Newt}} t) \left[1 - \frac{1}{2}\omega_{\text{Newt}}^2 t^2 + \mathcal{O}(\omega_{\text{Newt}}^4 t^4) \right]. \quad (\text{A4})$$

Obviously, this is the same as simply Taylor-expanding v_{los} to leading order.

One effect of the COM velocity drift is a Doppler shift to the waveform. Special relativity predicts that if a frequency source is moving with velocity v away from the observer at an angle θ , then the frequency observed is

$$\begin{aligned} \omega' &= \frac{\omega}{\Gamma} (1 + v \cos\theta)^{-1}, \\ &\sim \omega \left[1 - v \cos\theta + v^2 \left(\cos^2\theta - \frac{1}{2} \right) + \mathcal{O}(v^4) \right] \end{aligned} \quad (\text{A5})$$

where ω is the frequency of the source, ω' is the frequency the observer detects and $\Gamma = (1 - v^2)^{-1/2}$ is the usual special relativity factor. In the notation of Sec. II, $v \cos\theta = v_{\text{los}}$.

The Doppler shift effect can also be understood in two additional, complementary ways. The LISA response function naturally contains a Doppler shift term in the phase, due to LISA's motion about the Solar System barycenter. The Doppler shift discussed above is identical to this, but now it is the GW source that moves, as opposed to the detector. Similarly, one could consider first the GW phase emitted in the EMRI's center of mass, and then map this to that observed in the Solar System by shifting the phase's time-dependence by dt , corresponding to the light travel time along the line of sight between the center of mass of the EMRI system and the SMBH-SMBH system. From this perspective, the maximum phase shift that could accumulate in one year is simply the product of the EMRI orbital frequency and the light-crossing time of the projection of one year of SMBH binary evolution along the line of sight.

We can then easily integrate Eq. (A5), assuming a constant ω , to recover the $\Delta\Phi_{\text{GW}}$ computed in Sec II. Setting

$\iota = \pi/2 = \delta$, we find

$$\Delta\Phi_{\text{GW}} = -\omega \int v_{\text{los}}(t)dt, \sim -\frac{N}{2} \left(\frac{M_{\text{Sec}}}{M_{\text{Tot}}} \right) v_{\text{Newt}} (\omega_{\text{Newt}} T). \quad (\text{A6})$$

Notice that by choosing $\delta = \pi/2$, there is no leading-order, unobservable constant velocity drift term. In the

second line, we have Taylor expanded about $\omega_{\text{Newt}} t = 0$ and used that $\Phi_{\text{GW,Tot}} = N = \omega T$, where T is the time of integration, and that $\Phi_{\text{GW,Tot}} = N$, where N is the total number of radians in the non-accelerating waveform. Notice that this is the same $\Delta\Phi_{\text{GW}}$ correction described in Sec. II.

-
- [1] M. C. Miller et al., *ApJ Letters* **631**, L117 (2005).
[2] Y. Levin, *Mon. Not. Roy. Astron. Soc.* **374**, 515 (2007), astro-ph/0603583.
[3] P. Amaro-Seoane et al., *Class. Quantum Grav.* **24**, 113 (2007).
[4] S. A. Hughes, *Phys. Rev.* **D61**, 084004 (2000).
[5] S. A. Hughes, *Phys. Rev.* **D64**, 064004 (2001).
[6] L. Barack and C. Cutler, *Phys. Rev.* **D69**, 082005 (2004), gr-qc/0310125.
[7] S. Babak, H. Fang, J. R. Gair, K. Glampedakis, and S. A. Hughes, *Phys. Rev.* **D75**, 024005 (2007).
[8] N. Yunes, A. Buonanno, S. A. Hughes, and Y. Miller, M. C. and Pan, *Phys. Rev. Lett.* **104**, 091102 (2010), 0909.4263.
[9] N. Yunes, *GW Notes*, Vol. 2, p. 3-47 **2**, 3 (2009).
[10] N. Yunes, A. Buonanno, S. A. Hughes, Y. Pan, E. Barausse, M. C. Miller, and W. Throwe, *ArXiv e-prints* (2010), 1009.6013.
[11] G. Giampieri (1993), astro-ph/9305034.
[12] S. K. Chakrabarti, *Phys. Rev.* **D53**, 2901 (1996), astro-ph/9603117.
[13] R. Narayan, *The Astrophysical Journal* **536**, 663 (2000), arXiv:astro-ph/9907328.
[14] E. Barausse and L. Rezzolla, *Phys. Rev. D* **77**, 104027 (2008), 0711.4558.
[15] G. Hobbs, A. Archibald, Z. Arzoumanian, D. Backer, M. Bailes, N. D. R. Bhat, M. Burgay, S. Burke-Spolaor, D. Champion, I. Cognard, et al., *Classical and Quantum Gravity* **27**, 084013 (2010), 0911.5206.
[16] A. Buonanno and T. Damour, *Phys. Rev.* **D59**, 084006 (1999).
[17] A. Buonanno and T. Damour, *Phys. Rev.* **D62**, 064015 (2000).
[18] T. Damour, P. Jaranowski, and G. Schaefer, *Phys. Rev.* **D62**, 084011 (2000).
[19] T. Damour, *Phys. Rev.* **D64**, 124013 (2001).
[20] A. Buonanno, Y. Chen, and T. Damour, *Phys. Rev.* **D74**, 104005 (2006).
[21] T. Damour, P. Jaranowski, and G. Schaefer, *Phys. Rev.* **D78**, 024009 (2008), 0803.0915.
[22] E. Barausse and A. Buonanno, *Phys. Rev.* **D81**, 084024 (2010), 0912.3517.
[23] A. Nagar, T. Damour, and A. Tartaglia, *Class. Quant. Grav.* **24**, S109 (2007), gr-qc/0612096.
[24] T. Damour and A. Nagar, *Phys. Rev.* **D76**, 064028 (2007).
[25] S. Bernuzzi and A. Nagar, *Phys. Rev.* **D81**, 084056 (2010), 1003.0597.
[26] T. Damour, B. R. Iyer, and B. S. Sathyaprakash, *Phys. Rev.* **D57**, 885 (1998).
[27] T. Damour, B. R. Iyer, and A. Nagar, *Phys. Rev.* **D79**, 064004 (2009).
[28] Y. Pan, A. Buonanno, R. Fujita, E. Racine, and H. Tagoshi (2010), 1006.0431.
[29] R. Fujita and B. R. Iyer (2010), 1005.2266.
[30] T. Damour and A. Nagar, *Phys. Rev.* **D79**, 081503 (2009).
[31] A. Buonanno et al., *Phys. Rev.* **D79**, 124028 (2009).
[32] Y. Pan et al., *Phys. Rev.* **D81**, 084041 (2010), 0912.3466.
[33] L. Barack and N. Sago, *Phys. Rev. Lett.* **102**, 191101 (2009), 0902.0573.
[34] T. Damour, *Phys. Rev.* **D81**, 024017 (2010), 0910.5533.
[35] J. M. Bardeen, W. H. Press, and S. A. Teukolsky, *Astrophys. J.* **178**, 347 (1972).
[36] L. Blanchet, *Living Rev. Rel.* **9**, 4 (2006), and references therein, gr-qc/0202016.
[37] P. Laguna, S. L. Larson, D. Spergel, and N. Yunes, *The Astrophysical Journal Letters* **715**, L12 (2010), 0905.1908.
[38] L. Barack and C. Cutler, *Phys. Rev. D* **70**, 122002 (2004), arXiv:gr-qc/0409010.
[39] E. Berti, A. Buonanno, and C. M. Will, *Phys. Rev. D* **71**, 084025 (2005), arXiv:gr-qc/0411129.
[40] B. J. Owen, *Phys. Rev.* **D53**, 6749 (1996).
[41] L. Lindblom, J. G. Baker, and B. J. Owen, *ArXiv e-prints* (2010), 1008.1803.
[42] N. Yunes, K. G. Arun, E. Berti, and C. M. Will, *Phys. Rev. D* **80**, 084001 (2009), 0906.0313.
[43] C. Cutler and M. Vallisneri, *Phys. Rev.* **D76**, 104018 (2007), 0707.2982.
[44] N. Yunes and F. Pretorius, *Phys. Rev. D* **80**, 122003 (2009), 0909.3328.
[45] R. Takahashi and T. Nakamura, *Progress of Theoretical Physics* **113**, 63 (2005), arXiv:astro-ph/0408547.
[46] E. F. Bell, S. Phleps, R. S. Somerville, C. Wolf, A. Borch, and K. Meisenheimer, *The Astrophysical Journal* **652**, 270 (2006), arXiv:astro-ph/0602038.
[47] J. M. Lotz, M. Davis, S. M. Faber, P. Guhathakurta, S. Gwyn, J. Huang, D. C. Koo, E. Le Floc'h, L. Lin, J. Newman, et al., *The Astrophysical Journal* **672**, 177 (2008), arXiv:astro-ph/0602088.
[48] M. Milosavljević and D. Merritt, *The Astrophysical Journal* **596**, 860 (2003), arXiv:astro-ph/0212459.
[49] X. Chen, P. Madau, A. Sesana, and F. K. Liu, *The Astrophysical Journal Letters* **697**, L149 (2009), 0904.4481.
[50] X. Chen, A. Sesana, P. Madau, and F. K. Liu (2010), 1012.4466.